Volume 8
Number 23
21 June 2020
Pages 4965–5168

Journal of Materials Chemistry B

Materials for biology and medicine

rsc.li/materials-b

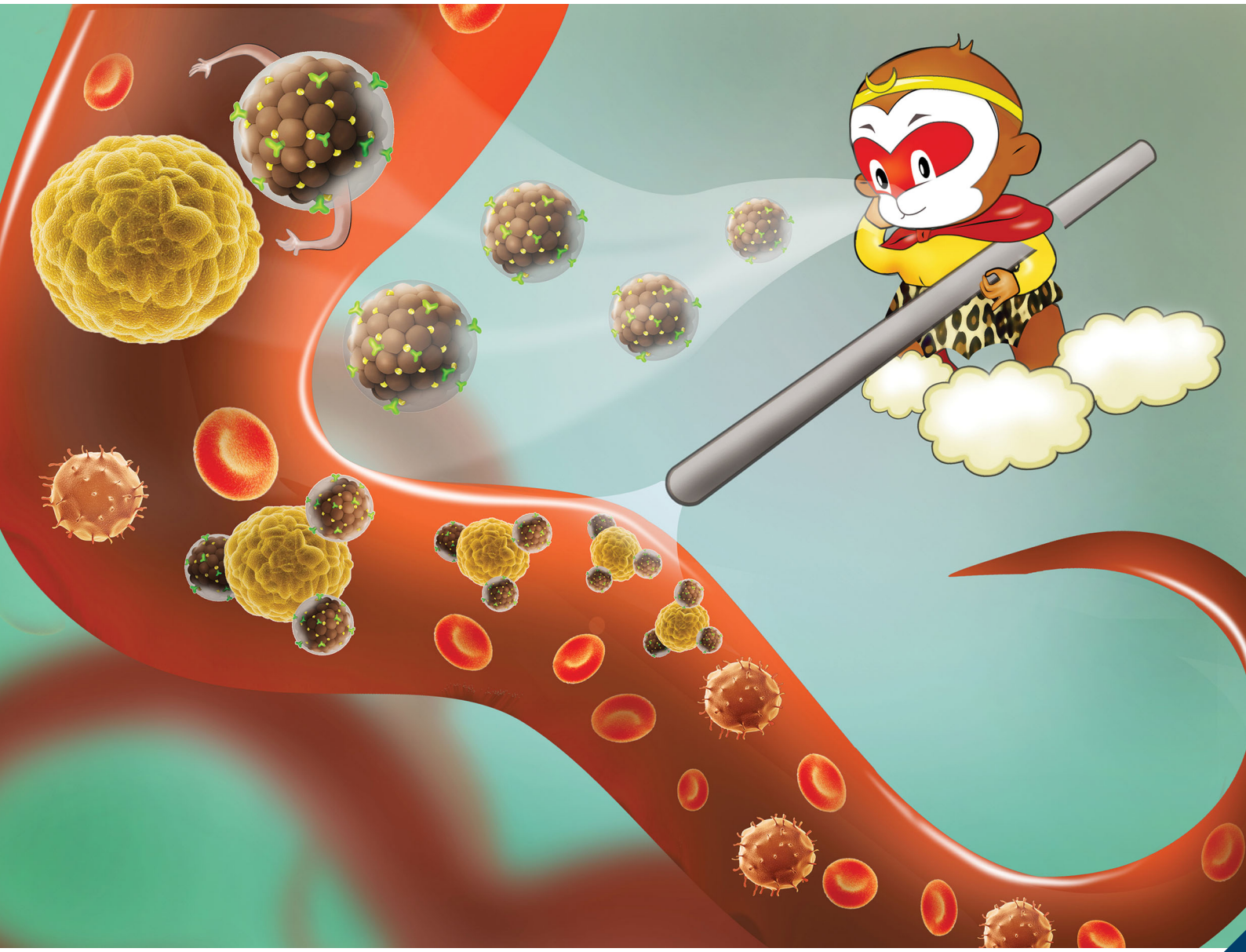

ISSN 2050-750X

ROYAL SOCIETY OF CHEMISTRY

PAPER

Wen-fei Dong, Zheng Wang *et al.*
Biomimetic immunomagnetic gold hybrid nanoparticles coupled with inductively coupled plasma mass spectrometry for the detection of circulating tumor cells

Indexed in Medline!

Journal of Materials Chemistry B

ROYAL SOCIETY OF CHEMISTRY

PAPER

View Article Online
View Journal | View Issue

Cite this: J. Mater. Chem. B, 2020, 8, 5019

Biomimetic immunomagnetic gold hybrid nanoparticles coupled with inductively coupled plasma mass spectrometry for the detection of circulating tumor cells†

Zhi-min Chang,[ab] Hang Zhou,[c] Chao Yang,[d] Rui Zhang,[b] Qiannan You,[b] Ruhong Yan,[b] Li Li,[b] Mingfeng Ge,[b] Yuguo Tang,[ab] Wen-fei Dong *[b] and Zheng Wang*[b]

Immunomagnetic beads are important tools for the isolation and detection of circulating tumor cells (CTCs). However, the current immunomagnetic bead technique provides poor CTC separation purity due to nonspecific binding of background cells. Furthermore, immunomagnetic beads have not been appropriately functionalized for enabling CTC analysis and quantification. In this work, bimetallic magnetic gold nanoparticles were prepared and coated with leukocyte membranes to form leukocyte membrane-camouflaged nanoparticles. After conjugation with the antibody of epithelial cell adhesion molecule (EpCAM), the biomimetic immunomagnetic gold nanoparticles (CM-Fe_3O_4@Au-Ab) showed a high specific recognition ability on mock (EpCAM-positive) CTCs and a reduced interaction with leukocytes. We subsequently optimized the conditions for CTC separation, including the concentration of nanoparticles and the incubation time. Under the optimized conditions, CM-Fe_3O_4@Au-Ab exhibited high CTC capture efficiency with negligible background cell binding in mock clinical blood samples. More importantly, gold probes were tagged on the surface of these separated CTCs. When coupled with ICP-MS analysis, the number of CTCs and gold signals exhibited a good linear relationship, and a low limit of detection was obtained, enabling us to estimate the number of CTCs in blood samples. Hence, we expected that CM-Fe_3O_4@Au-Ab could provide an opportunity to surmount the limitations of current CTC detection.

Received 13th February 2020,
Accepted 1st May 2020

DOI: 10.1039/d0tb00403k

rsc.li/materials-b

1. Introduction

Circulating tumor cells (CTCs), which detach from solid tumors and travel in the circulatory system, contain important information closely correlated with cancer progression.[1–5] The detection of CTCs is of proven great significance for early clinical diagnosis, metastatic malignancy examination and the prediction of patient prognosis.[6,7] Commonly, CTC detection involves two important steps: CTC enrichment and quantification.[8,9] However, CTCs are extremely rare in the peripheral blood, which leads to challenges for the specific separation of CTCs and accurate counting.[10,11] To date, numerous techniques have been developed for solving the abovementioned problems.[8,12–17] Among these approaches, immunomagnetic bead-based CTC enrichment, in which magnetic beads are conjugated with specific antibodies, is the focus of attention because of rapid magnetic isolation along with nanoscale advantages such as a high surface area, good biocompatibility and suspendability.[14,18–21] Although promising, immunomagnetic beads still have limitations. First, the nonspecific interaction of leukocytes with nanoparticles leads to a low separated purity, affecting the subsequent bioassay.[8,22,23] Furthermore, immunomagnetic beads have not been appropriately functionalized for enabling CTC analysis and quantification, resulting in subsequent tedious and time-consuming operations.[24] Hence, it is urgent to rationally design immunomagnetic nanoparticles with multiple functions to improve the specificity and sensitivity of CTC isolation as well as enable the counting of CTCs.[25]

Recently, inductively coupled plasma mass spectrometry (ICP-MS), which detects specific elements, has attracted

[a] Academy for Engineering & Technology, Fudan University, Shanghai 200433, China
[b] CAS Key Laboratory of Bio-Medical Diagnostics, Suzhou Institute of Biomedical Engineering and Technology, Chinese Academy of Sciences, Suzhou 215163, China
[c] Department of Ultrasound, The Second Affiliated Hospital, Zhejiang University School of Medicine, Hangzhou 310000, P. R. China
[d] Institutes of Life Sciences, School of Biomedical Sciences and Engineering and National Engineering Research Center for Tissue Restoration and Reconstruction, South China University of Technology, Guangzhou, Guangzhou International Campus, Guangdong 510006, China

† Electronic supplementary information (ESI) available. See DOI: 10.1039/d0tb00403k

intensive attention owing to its high sensitivity, low detection limits, wide linear range and rapid analysis abilities.[26,27] Compared with other detection techniques, ICP-MS based methods possess remarkable advantages. For example, ICP-MS methods perform less interference than electrochemical methods, are much simpler and shortage of sensitivity to light which allows for laboratory labelling under convenient ambient conditions in comparison to flow cytometry.[28,29] Among various elemental tags, gold nanoparticles have been considered ideal probes in ICP-MS measurements because of their high atomic number, stable property, good biocompatibility and easily functionalized surface.[30] Zhang *et al.*[31] prepared magnetic nanoprobes and gold nanoprobes and utilized the two probes to capture and detect CTCs. However, it appears to be more promising to combine the functions of CTC separation and detection into a single nanostructure. Furthermore, the low purity resulting from the nonspecific adsorption of background cells has not yet been properly addressed.

Magnetic–gold hybrid nanoparticles are the focus of attention due to their excellent biocompatibility and unique physicochemical properties.[32] Bimetallic nanoparticles have been shown to have potential applications in drug delivery, multimodal therapies and imaging.[33–35] Nevertheless, potential applications for CTC detection have not yet been reported. In addition, considering the unsatisfactory separation purity of CTCs, additional techniques should be employed to enhance the specific recognition capability of nanoparticles to CTCs and to decrease nonspecific interactions with blood cells.[25] Recent studies have revealed that a leukocyte membrane coating on nanoparticles can effectively inhibit the binding of blood cells with nanoparticles, taking advantage of the feature that homologous leukocytes do not form clusters in the circulatory system.[36–39]

Hence, in the present study, biomimetic magnetic–gold nanoparticles were designed for high-specificity CTC capture and analysis (Scheme 1). The bimetallic nanoparticles (Fe_3O_4@Au) contained a Fe_3O_4 core with superior magnetic responsiveness and a gold shell as an elemental tag for ICP-MS detection.[27] The leukocyte membrane (CM) was coated on the surface of hybrid nanoparticles to form CM-Fe_3O_4@Au, and subsequently, an epithelial cell adhesion molecule (EpCAM) antibody (Ab) was modified on the surface of CM-Fe_3O_4@Au (CM-Fe_3O_4@Au-Ab) to enhance the specificity to CTCs. CM-Fe_3O_4@Au-Ab exhibited excellent targeting to MCF-7 breast cancer cells from mock clinical blood samples and a reduced interaction with background cells. More importantly, a good linear relationship between the gold signal and the number of CTCs was obtained. Hence, high-efficiency isolation of CTCs and accurate ICP-MS measurement were simultaneously realized by this single biomimetic nanoparticle, which provided a feasible strategy for CTC detection in the clinic.

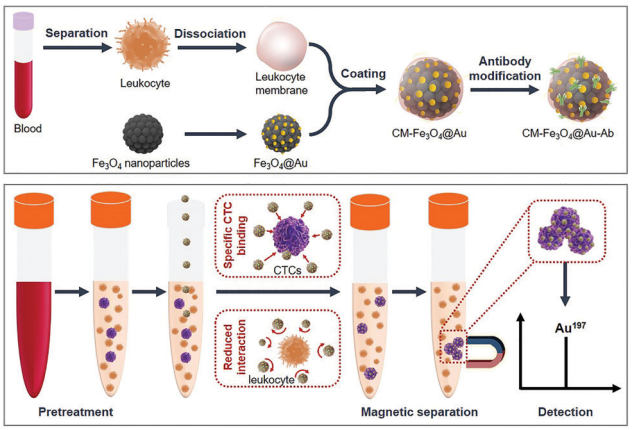

Scheme 1 Schematic of the preparation of CM-Fe_3O_4@Au-Ab for high-purity CTCs isolation and ICP-MS analysis.

2. Experimental

2.1 Synthesis of Fe_3O_4@Au

Polyacrylic acid (PAA)-stabilized Fe_3O_4 NPs were synthesized by a high-temperature hydrolysis reaction.[13,40,41] Then, 0.2 g of 3-mercaptopropyltrimethoxysilane (MPTMS) and 0.5 ml of ammonia aqueous (NH_4OH) were successively injected into a 10 ml solution of PAA-stabilized Fe_3O_4 NPs (1 mg ml^{-1}). After stirring for 24 h, SH-functionalized Fe_3O_4 NPs (Fe_3O_4-SH) were obtained. To form core–shell Fe_3O_4@Au, 1 ml of tetrachloroauric acid ($HAuCl_4$) (0.01 M) was dispersed in 30 ml of pure water. Then, 10 ml of Fe_3O_4-SH NPs (1 mg ml^{-1}) was mixed with the above solution, and 0.01 M sodium hydroxide (NaOH) was used to adjust the pH to 9. After 30 min of stirring and dialysis, 6 mL of sodium borohydride ($NaBH_4$) (0.01 M) was slowly injected into the mixture and reacted for 6 h. Then, Au seeds attached to Fe_3O_4 (Au-Fe_3O_4) were obtained after centrifugation and magnetic separation. To form a gold shell, 50 ml of potassium carbonate (K_2CO_3) (0.2 mg ml^{-1}) was mixed with 2 ml of $HAuCl_4$ (0.01). Then, the prepared Au-Fe_3O_4 was added into the mixture, followed by 0.5 ml of L-ascorbic acid. After 10 min, Fe_3O_4@Au was obtained through centrifugation and magnetic separation.

2.2 Preparation of CM-Fe_3O_4@Au

Leukocytes were isolated from blood samples and enucleated in an IKA T18 basic homogenizer.[42,43] Then, the supernatants were collected and suspended in 1 ml of water. After 10 min of sonicating, the mixture was extruded through 200 nm polycarbonate membranes by an Avanti Mini-Extruder (Avanti Polar Lipids). The obtained cell membranes (CM) were stored at 4 °C for further use. To form CM-Fe_3O_4@Au, Fe_3O_4@Au was mixed with CM under sonication for 5 min. Then, the mixture was extruded through 200 nm polycarbonate membranes to form CM-Fe_3O_4@Au.[44,45]

2.3 Preparation of CM-Fe_3O_4@Au-Ab

First, 100 μl of a 4-morpholineethanesulfonic acid (MES) buffer solution of 1-ethyl-3-(3-dimethylaminopropyl)carbodiimide hydrochloride (EDC) (4 mg ml^{-1}) and 100 μl of a MES buffer solution of *N*-hydroxysuccinimide (NHS) (6 mg ml^{-1}) were added into a solution of CM-Fe_3O_4@Au. After 30 min of stirring at room temperature, the mixture was washed with PBS three times, and then, the mixture was treated with a certain amount of

streptavidin (50 μg ml^{-1} Phosphate buffer saline (PBS)) for 10 h. Next, 1 mg of anti-EpCAM was added to the mixture and reacted at room temperature for 2 h. After washing with PBS and centrifugation at 8000 rpm for 10 min repeatedly, the purified CM-Fe_3O_4@Au-Ab was obtained.

2.4 Cell culture and cytotoxicity

MCF-7 cells and leukocytes were cultured with RPMI-1640 medium containing 10% fetal bovine serum (FBS) at 37 °C and 5% CO_2. The cytotoxicity was determined by sulforhodamine B (SRB) assay. Briefly, these cells were seeded on a 96-well plate. Then, various concentrations (6.25, 12.5, 25, 50, 100, 150 and 200 μg mL^{-1}) of CM-Fe_3O_4@Au-Ab were incubated with these cells for 24 h, and 100 mL of 20% trichloroacetic acid was subsequently added to the cells. After 3 h, the supernatant was removed, and 100 mL of 0.4% w/v SRB solution was added. After 30 min of incubation, 150 mL of Tris (hydroxymethyl) aminomethane Hydrochloride (Tris–HCl) was added to solubilize SRB. The OD value was recorded, and the cell viability was calculated.

2.5 Investigation of the specific recognition of CM-Fe_3O_4@Au-Ab with epithelial cancer cells

Fe_3O_4@Au-Ab, Fe_3O_4@Au, CM-Fe_3O_4@Au-Ab and CM-Fe_3O_4@Au (50 μg mL^{-1}) were separately incubated with 1×10^5 MCF-7 cells and Jurkat T cells for 20 min at 4 °C. In addition, CM-Fe_3O_4@Au-Ab or Fe_3O_4@Au-Ab (50 μg mL^{-1}) was incubated with 1 mM free anti-EpCAM to block MCF-7 cells. Then, the cells binding to these nanoparticles were captured by an external magnet. We used a small NdFeB permanent magnets (5 mm × 3 mm × 2 mm cylinder, surface magnetic field of 0.2 T) as the external magnet and the magnet was placed besides the tube for 5 minutes. Then, the separated cells were counted by a hemocytometer to calculate the capture efficacy. In addition, the cells were observed by scanning electronic microscopy (SEM). To optimize the incubation concentration, various concentrations (3.125, 6.25, 12.5, 25, 50, and 100 μg mL^{-1}) of CM-Fe_3O_4@Au-Ab were incubated with 1×10^5 MCF-7 cells for 30 min. To optimize the incubation time, 50 μg mL^{-1} of CM-Fe_3O_4@Au-Ab were incubated with 1×10^5 MCF-7 cells for 5 min, 15 min, 20 min, 25 min 30 min, 40 min and 60 min. Then, the separated cells were counted to calculate the capture efficacy. To research the capture ability of CM-Fe_3O_4@Au-Ab towards various concentration of MCF-7 cells, MCF-7 cells ranging from 100 to 5000 with were resuspended in 5 ml of PBS solution. Then, 50 μg mL^{-1} of various nanoparticles were added into the synthetic samples and incubated for 20 min. After magnetic separation, the number of MCF-7 cells were counted.

2.6 Investigation of the interaction of CM-Fe_3O_4@Au-Ab with leukocytes

The leukocytes were isolated from human blood *via* gradient centrifugation. Briefly, 1 mL healthy human blood was mixed with 1 mL Hank's balanced salt solution, then the mixture was added into 2 mL of lymphocyte separation medium. Followed by centrifugation at room temperature at 1800 rpm for 30 min. Top layer of plasma was collected and the white mononuclear cells and the supernatant at the middle position was re-suspended in Hank's balanced salt solution and centrifuged at 2000 rpm for 10 min. A total of 1×10^5 leukocytes was incubated with 50 μg mL^{-1} CM-Fe_3O_4@Au-Ab and Fe_3O_4@Au-Ab for 20 min. Then, the mixture was centrifuged at 2000 rpm for 2 min. After discarding the supernatant for removing the unbound nanoparticles, the cells binding to the nanoparticles were observed by SEM, and the Fe content was measured by ICP-MS (Optima 5300DV, PerkinElmer, USA). To investigate the cell capture purity in synthetic CTC blood samples, 5×10^3 of MCF-7 cells were spiked into 1 mL of RBC-lysed healthy human blood. Then, 50 μg mL^{-1} CM-Fe_3O_4@Au-Ab or Fe_3O_4@Au-Ab was added to the synthetic samples and co-incubated for 20 min. After magnetic separation, the captured cells were stained with 10 μL of FITC-anti-CD45 and PE-anti-CK stock solutions at 4 °C for 1 h. Finally, these cells were quantified by flow cytometry for analyzing the separation purity.

2.7 CTC analytic performance

To investigate the detection of CTCs in blood, Hoechst 33342-stained MCF-7 cells ranging from 100 to 5000 were spiked in 5 ml of RBC-lysed human blood. Next, 50 μg mL^{-1} CM-Fe_3O_4@Au-Ab or Fe_3O_4@Au-Ab was added to the synthetic samples. After 20 min of incubation, these cells were separated by an external magnet, and the number of MCF-7 cells was quantified by flow cytometry. The gold content binding with the cells was counted. Then, unbound CM-Fe_3O_4@Au-Ab was removed by filtration, and the gold content was detected by ICP-MS.

2.8 Statistical analyses

Bonferroni *post hoc* tests and one-way analysis of variance were carried out to analyze the differences between the two groups. $P < 0.05$ represented a significant difference.

3. Results and discussions

The bimetallic superparamagnetic–gold nanoparticles (Fe_3O_4@Au) were synthesized by a gold seed growth method using thiol-functionalized Fe_3O_4 as a substrate, $HAuCl_4$ along with $NaBH_4$ to form gold seeds to attach the surface of Fe_3O_4, and $HAuCl_4$ and L-ascorbic acid to further form the gold shells.

As shown in Fig. 1a, Fe_3O_4@Au exhibited a uniform spherical structure consisting of a core with a diameter of approximately 80 nm and a shell with a thickness of approximately 20 nm. The energy-dispersive X-ray spectrum in Fig. S1 (ESI†) further demonstrated the existence of iron and oxygen as well as gold. Then, leukocyte membrane vesicles (CMVs) were extracted from leukocytes and coated on the surface of Fe_3O_4@Au to form CM-Fe_3O_4@Au. The TEM images in Fig. 1b clearly present the outline of slight gray cell membranes around the Fe_3O_4@Au particles. The *Z*-average size of CM-Fe_3O_4@Au was 121 nm, higher than that of Fe_3O_4@Au in Fig. 1c. Moreover, the ζ potential of CM-Fe_3O_4@Au was −17.3 mV, which was approximate to the CMV and lower than that of Fe_3O_4@Au (Fig. 1c), further confirming that Fe_3O_4@Au was successfully coated by the CMVs.

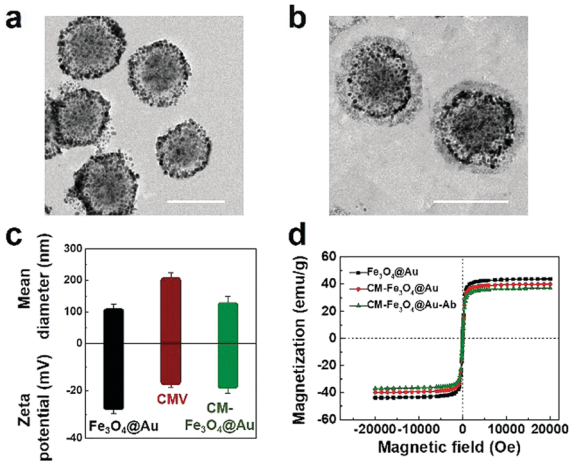

Fig. 1 Characterization of CM-Fe_3O_4@Au. TEM images (a) Fe_3O_4@Au (scale bar = 100 nm) and (b) CM-Fe_3O_4@Au (scale bar = 100 nm), (c) the *Z*-average size and zeta potential of Fe_3O_4@Au, CMV, and CM-Fe_3O_4@Au measured by DLS. Data represent the mean ± s.d. (n = 5), (d) magnetization curve of Fe_3O_4@Au, CM-Fe_3O_4@Au and CM-Fe_3O_4@Au-Ab.

To enable CM-Fe_3O_4@Au specifically recognizing CTCs, anti-epithelial cell adhesion molecules (Abs) were conjugated on the surface of CM-Fe_3O_4@Au. The UV-vis spectrum shown in Fig. S2 (ESI†) confirmed the successful modification of Ab onto CM-Fe_3O_4@Au, as indicated by the characteristic absorption peak of anti-EpCAM at 280 nm in CM-Fe_3O_4@Au-Ab. Notably, this facile modification surface was promising for the conjugation with other anti-bodies, which would expand their broad application on detecting other type of cells. The saturation magnetization value of CM-Fe_3O_4@Au-Ab reached a maximum of 36 emu g^{-1}, which was similar to that of CM-Fe_3O_4@Au and Fe_3O_4@Au, indicating that the coating of CM and the modification of Ab barely affected the magnetic properties of the nanoparticles (Fig. 1d). The photo images in Fig. S3 (ESI†) show that CM-Fe_3O_4@Au-Ab could be collected and retrieved from PBS solution for 2 min under an external magnetic field. The excellent magnetic response of these nanoparticles indicated a rapid CTC collection capability. Then, we investigated the biosafety of CM-Fe_3O_4@Au-Ab. As shown in Fig. S4 (ESI†), no obvious cytotoxicity was detected in MCF-7 cells and leukocytes even when the concentration of CM-Fe_3O_4@Au-Ab reached 100 μg ml^{-1}, indicating that these nanoparticles possessed good biocompatibility.

To research the specificity of CM-Fe_3O_4@Au-Ab to recognize epithelial cancer cells, we employed MCF-7 cells overexpressing EpCAM as a positive control and Jurkat T cells with low expression of EpCAM as a negative control. As shown in Fig. 2a, Fe_3O_4@Au exhibited a low capture efficiency towards MCF-7 cells and Jurkat T cells. 79% of MCF-7 cells were captured by CM-Fe_3O_4@Au-Ab, which was similar to that by Fe_3O_4@Au-Ab, whereas only 15% of Jurkat T cells could be separated. CM-Fe_3O_4@Au had a similar capture ratio in the two types of cells, which was much lower than the efficiency of CM-Fe_3O_4@Au-Ab in capturing MCF-7 cells. Notably, the capture efficiency of CM-Fe_3O_4@Au-Ab was significantly attenuated when 1 mM free anti-EpCAM was preincubated

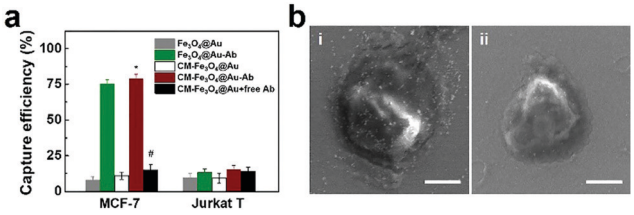

Fig. 2 Specific capture of MCF-7 cells. (a) The capture efficiency of MCF-7 cells and Jurkat T cells in PBS by using various nanoparticles. Data represent the mean ± s.d. (n = 5). $^{*}P < 0.05$ *versus* Fe_3O_4@Au group, $^{\#}P < 0.05$ *versus* CM-Fe_3O_4@Au-Ab group. (b) SEM images of MCF-7 cell (i) and Jurkat T cell (ii) binding with CM-Fe_3O_4@Au-Ab (scale bar = 5 μm).

with the MCF-7 cells (Fig. 2a). The scanning electron microscopy (SEM) images in Fig. 2b show that numerous CM-Fe_3O_4@Au-Ab adhered onto the MCF-7 cells, whereas a lower number of CM-Fe_3O_4@Au-Ab was observed on the Jurkat T cells. Furthermore, CM-Fe_3O_4@Au-Ab also exhibited high capture efficiency on other cancer cell lines with overexpressing EpCAM, such as HCT116 cell lines, whereas for EpCAM-negative HeLa cells, the capture efficiencies of CM-Fe_3O_4@Au-Ab was less than 15% (Fig. S5, ESI†). These results confirmed that CM-Fe_3O_4@Au-Ab possessed a specific binding capacity with epithelial cancer cells due to anti-EpCAM modification, indicating the excellent potency of CM-Fe_3O_4@Au-Ab in capturing CTCs because EpCAM is overexpressed in most CTCs.

To achieve the best CTC capture efficiency, the experimental parameters were optimized including the concentration of CM-Fe_3O_4@Au-Ab and incubation time. As shown in Fig. 3a, the capture efficiency of CM-Fe_3O_4@Au-Ab exhibited a concentration-dependent increase. When the concentration of Fe_3O_4@Au-Ab was above 50 μg mL^{-1}, the number of separated MCF-7 cells no longer increased. The capture efficiency also increased with increasing incubation time within 20 min (Fig. 3b), indicating that the specific binding of CM-Fe_3O_4@Au-Ab with CTCs was completed in 20 min. Thus, 50 μg mL^{-1} CM-Fe_3O_4@Au-Ab and 20 min of incubation time were used in the subsequent assay. To evaluate the capture ability of CM-Fe_3O_4@Au-Ab, various number of MCF-7 cells were dispersed into the PBS solution and the 50 μg mL^{-1} of nanoparticles were added for 20 min incubation for detecting the capture efficiency. As shown in Fig. 3c, both CM-Fe_3O_4@Au-Ab and Fe_3O_4@Au-Ab showed a high capture efficiency to various concentration of MCF-7 cells,

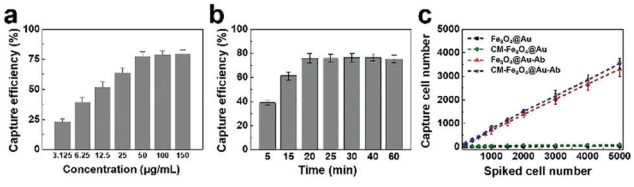

Fig. 3 The capture efficiency of MCF-7 cells. (a) Capture efficiencies of MCF-7 cells with various concentrations of CM-Fe_3O_4@Au-Ab, (b) efficiencies of separating MCF-7 cells by 50 μg mL^{-1} CM-Fe_3O_4@Au-Ab with different incubation times. (c) The number of MCF-7 cells captured in PBS solutions with various concentrations of MCF-7 cells. Data represent the mean ± s.d. (n = 5).

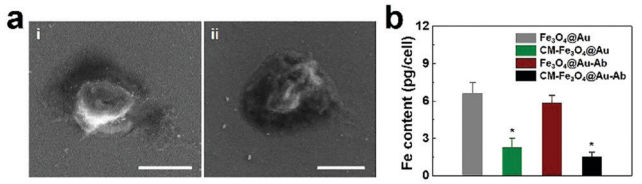

Fig. 4 The reduced nonspecific adsorption of CM-Fe_3O_4@Au-Ab with leukocytes. (a) SEM images of leukocytes interacting with Fe_3O_4@Au-Ab (i) and CM-Fe_3O_4@Au-Ab (ii) (scale bar = 10 μm). (b) ICP-MS analysis of Fe content in leukocytes after treatment with various nanoparticles. Data represent the mean ± s.d. (n = 5), *P < 0.05 *versus* Fe_3O_4@Au group.

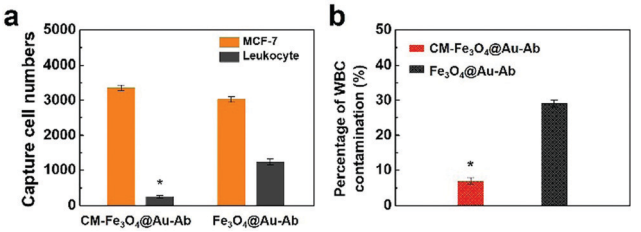

Fig. 5 (a) Flow cytometry analysis of separated cells from spiked blood samples by CM-Fe_3O_4@Au-Ab and Fe_3O_4@Au-Ab. Data represent the mean ± s.d. (n = 3), *P < 0.05 *versus* Fe_3O_4@Au group. (b) The percentage of leukocytes in the captured cells by CM-Fe_3O_4@Au-Ab and Fe_3O_4@Au-Ab. Data represent the mean ± s.d. (n = 3), *P < 0.05 *versus* Fe_3O_4@Au group.

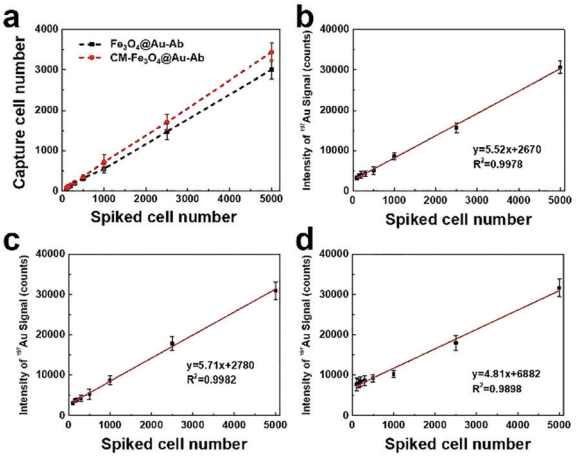

Fig. 6 Analytical performance of CM-Fe_3O_4@Au-Ab coupled with ICP-MS detection. (a) The number of MCF-7 cells captured in blood spiked with different numbers of MCF-7 cells. Calibration of the number of spiked MCF-7 cells and gold signals after CM-Fe_3O_4@Au-Ab-tagged immunomagnetic separation in the blood samples spiked with MCF-7 cells (b) and the PBS solutions of pure MCF-7 cells (c). Calibration of the number of spiked MCF-7 cells and gold signals after Fe_3O_4@Au-Ab tagged immunomagnetic separation in the blood samples spiked with MCF-7 cells (d). Data represent the mean ± s.d. (n = 5).

whereas negligible MCF-7 cells were separated by CM-Fe_3O_4@Au and Fe_3O_4@Au, which confirmed that CM-Fe_3O_4@Au-Ab possessed high recognition ability due to Ab modification.

An ideal agent for CTC capture should be qualified with not only specific CTC recognition but also high CTC separation purity. We proposed that the coated leukocyte membranes could effectively inhibit the nonspecific adsorption of leukocytes. To validate this hypothesis, we incubated leukocytes with different nanoparticles and explored their interaction. As shown in Fig. 4a, a number of Fe_3O_4@Au-Ab nanoparticles adhered to leukocytes, whereas CM-Fe_3O_4@Au-Ab exhibited less adsorption with leukocytes. The ICP-MS analysis in Fig. 4b shows a high content of iron in the washed leukocytes after coincubation with Fe_3O_4@Au-Ab and Fe_3O_4@Au. In contrast, the iron content was lower in those samples treated with CM-Fe_3O_4@Au-Ab and CM-Fe_3O_4@Au. These results demonstrated that the coating of cell membranes on the surface of the nanoparticles could effectively weaken the adsorption of leukocytes to the nanoparticles. The membrane protein CD47 on leukocytes is reported to functions as a marker to impedes phagocytosis of self by signaling through the leukocyte receptor CD172a. Our biomimetic magnetosomes, due to the reserved antigens and membrane structure from the leukocyte, would be repelled when it encountered humongous leukocytes, which was conducive to achieving high-purity CTC capture. We believe the cell membrane-cloaked strategy will be likewise applicable to other CTC techniques such as microfluidic chip techniques to improve separation purity of CTCs.[46,47] To further investigate the separation purity of these nanoparticles, a concentration of 5×10^3 cells per mL of MCF-7 was spiked into human RBC-lysed blood to mimic clinical CTC-containing blood samples. Then, we quantified the separated cells by flow cytometry. As shown in Fig. 5a, an average of 3022 MCF-7 cells were captured by Fe_3O_4@Au-Ab along with more than 1100 leukocytes. Encouragingly, CM-Fe_3O_4@Au-Ab averagely captured 3349 MCF-7 cells and 254 leukocytes. The percentage of leukocytes in the captured cells by CM-Fe_3O_4@Au-Ab (7.1%) was less than that by Fe_3O_4@Au-Ab (29.1%) (Fig. 5b). The results were encouraging because current magnetism-activated cell sorting (MACS) beads suffer from nonspecific interactions with leukocytes, leading to inaccuracies and limitations in CTC detection. Our CM-Fe_3O_4@Au-Ab with high separation purity might facilitate the subsequent bioassay.

To evaluate the isolation capacity and analytical performance of CM-Fe_3O_4@Au-Ab in real bloods, a certain number of MCF-7 cells ranging from 100–5000 were spiked into the human healthy blood samples. As shown in Fig. 6a, CM-Fe_3O_4@Au-Ab showed a superb capture ratio with the increased cell number, which was approximate to Fe_3O_4@Au-Ab. Then, the separated cells were filtered for the removal of unbound CM-Fe_3O_4@Au-Ab and subsequently subjected to ICP-MS analysis. As shown in Fig. 6b, the number of spiked MCF-7 cells by CM-Fe_3O_4@Au-Ab and gold signal intensity presented a good linear relationship ($y = 5.52x + 2670$, $R^2 = 0.9978$). The limit of detection (LOD) was calculated to be 83 according to the equation LOD = $3\sigma/k$, in which σ represented the standard deviation of blank experiment and k means the slope. It is worth mentioning that the concentrations of CTCs in clinical blood samples are much lower than that LOD. Nevertheless, the LOD of our CM-Fe_3O_4@Au-Ab-based ICP-MS was lower than other methods such as some cytosensors and electrochemical detection.[31,48–50] Hence, when combined with signal amplification technique, our CM-Fe_3O_4@Au-Ab would provide a more

sensitive CTC detection. Notably, the linear relationship between the number of spiked MCF-7 cells by CM-Fe_3O_4@Au-Ab and gold signal intensity as well as LOD in blood samples were approximate to that in a PBS solution of pure MCF-7 cells ($y = 5.71x + 2780$, $R^2 = 0.9982$, LOD = 78, Fig. 6c). Conversely, Fe_3O_4@Au-Ab exhibited a different equation and poor linear relationship in blood samples ($y = 4.81x + 6882$, $R^2 = 0.9898$, LOD = 121) compared with CM-Fe_3O_4@Au-Ab (Fig. 6d). This difference was because the cells captured by Fe_3O_4@Au-Ab contained a number of leukocytes, which led to a part of the signal intensity being from leukocytes. These results demonstrated that CM-Fe_3O_4@Au-Ab possessed better analytical performance than Fe_3O_4@Au-Ab due to their small interferences with components existing in the blood, especially confounding leukocytes, suggesting excellent potential for the clinical detection of CTCs. In the future, we will combine some signal technique of ICP-MS to quantify CTCs in the blood of cancer patient for predicting the cancerous progress.

4. Conclusions

In summary, biomimetic immunomagnetic–gold nanoparticles (CM-Fe_3O_4@Au-Ab) were designed to capture and analyze CTCs. CM-Fe_3O_4@Au-Ab with uniform morphology possessed stable physicochemical properties and rapid magnetic responsiveness as well as excellent biocompatibility. We revealed the anti-EpCAM-mediated recognition of CM-Fe_3O_4@Au-Ab by CTCs and their reduced interaction with leukocytes due to the modification of cell membranes. After optimizing the parameters, CM-Fe_3O_4@Au-Ab exhibited high specificity and sensitivity for capturing CTCs. More importantly, a good linear relationship between the number of CTCs and gold signal intensity was obtained by ICP-MS analysis, which enabled accurate quantification of CTCs. Our research revealed the potency of bimetallic magnetic–gold nanoparticles in CTC detection and provided a feasible approach to simultaneously achieve rapid CTC collection and analysis by a single agent.

Conflicts of interest

There are no conflicts to declare.

Acknowledgements

This work was supported by the National Natural Science Foundation of China (Grand No. 81902166, 81771982, 61535010, 8160071152 and 21803075), the National Key R&D Program of China (Grand No. 2017YFF0108600 and 2017YFC0211900), the Natural Science Foundation of Jiangsu Province (No. BK20181236 and BE2019683), the Primary Research & Development Plan of Jiangsu Province (BE2019683) and the Science and Technology Department of Jinan City (2018GXRC016).

References

1 M.-Y. Kim, T. Oskarsson, S. Acharyya, D. X. Nguyen, X. H.-F. Zhang, L. Norton and J. Massagué, *Cell*, 2009, **139**, 1315–1326.
2 C. L. Chaffer and R. A. Weinberg, *Science*, 2011, **331**, 1559–1564.
3 J. D. Cohen, A. A. Javed, C. Thoburn, F. Wong, J. Tie, P. Gibbs, C. M. Schmidt, M. T. Yip-Schneider, P. J. Allen and M. Schattner, *Proc. Natl. Acad. Sci. U. S. A.*, 2017, **114**, 10202–10207.
4 M. Cristofanilli, G. T. Budd, M. J. Ellis, A. Stopeck, J. Matera, M. C. Miller, J. M. Reuben, G. V. Doyle, W. J. Allard and L. W. Terstappen, *N. Engl. J. Med.*, 2004, **351**, 781–791.
5 P. Paterlini-Brechot and N. L. Benali, *Cancer Lett.*, 2007, **253**, 180–204.
6 C. Alixpanabieres and K. Pantel, *Nat. Rev. Cancer*, 2014, **14**, 623–631.
7 C. Alixpanabieres and K. Pantel, *Klin. Lab. Diagn.*, 2014, 60.
8 Z. Shen, A. Wu and X. Chen, *Chem. Soc. Rev.*, 2017, **46**, 2038–2056.
9 E. I. Galanzha, E. V. Shashkov, T. Kelly, J.-W. Kim, L. Yang and V. P. Zharov, *Nat. Nanotechnol.*, 2009, **4**, 855.
10 V. Plaks, C. D. Koopman and Z. Werb, *Science*, 2013, **341**, 1186–1188.
11 T. M. Gorges and K. Pantel, *Cancer Immunol. Immunother.*, 2013, **62**, 931–939.
12 C. Wang, M. Ye, L. Cheng, R. Li, W. Zhu, Z. Shi, C. Fan, J. He, J. Liu and Z. Liu, *Biomaterials*, 2015, **54**, 55–62.
13 Z.-m. Chang, Z. Wang, D. Shao, J. Yue, H. Xing, L. Li, M. Ge, M. Li, H. Yan and H. Hu, *ACS Appl. Mater. Interfaces*, 2018, **10**, 10656–10663.
14 C.-Y. Wen, L.-L. Wu, Z.-L. Zhang, Y.-L. Liu, S.-Z. Wei, J. Hu, M. Tang, E.-Z. Sun, Y.-P. Gong and J. Yu, *ACS Nano*, 2014, **8**, 941–949.
15 H. Min, S. M. Jo and H. S. Kim, *Small*, 2015, **11**, 2536–2542.
16 S. Fang, C. Wang, J. Xiang, L. Cheng, X. Song, L. Xu, R. Peng and Z. Liu, *Nano Res.*, 2014, **7**, 1327–1336.
17 M. Alunni-Fabbroni and M. T. Sandri, *Methods*, 2010, **50**, 289–297.
18 J. Wu, X. Wei, J. Gan, L. Huang, T. Shen, J. Lou, B. Liu, J. X. Zhang and K. Qian, *Adv. Funct. Mater.*, 2016, **26**, 4016–4025.
19 Z. Wang, N. Sun, H. Liu, C. Chen, P. Ding, X. Yue, H. Zou, C. Xing and R. Pei, *ACS Appl. Mater. Interfaces*, 2019, **11**, 39586–39593.
20 B.-I. Haukanes and C. Kvam, *Bio/Technology*, 1993, **11**, 60–63.
21 M. Yu, S. Stott, M. Toner, S. Maheswaran and D. A. Haber, *J. Cell Biol.*, 2011, **192**, 373–382.
22 J. Clement, M. Schwalbe, N. Buske, K. Wagner, M. Schnabelrauch, P. Görnert, K. Kliche, K. Pachmann, W. Weitschies and K. Höffken, *J. Cancer Res. Clin. Oncol.*, 2006, **132**, 287–292.
23 M. Schwalbe, C. Jörke, N. Buske, K. Höffken, K. Pachmann and J. H. Clement, *J. Magn. Magn. Mater.*, 2005, **293**, 433–437.
24 K. C. Andree, G. Van Dalum and L. W. M. M. Terstappen, *Mol. Oncol.*, 2016, **10**, 395–407.

25 R. Harouaka, Z. Kang, S.-Y. Zheng and L. Cao, *Pharmacol. Ther.*, 2014, **141**, 209–221.
26 L. Cid-Barrio, F. Calderón-Celis, P. Abásolo-Linares, M. L. Fernández-Sánchez, J. M. Costa-Fernández, J. R. Encinar and A. Sanz-Medel, *TrAC, Trends Anal. Chem.*, 2018, **104**, 148–159.
27 A. A. Ammann, *J. Mass Spectrom.*, 2007, **42**, 419–427.
28 X. Li, B. Chen, M. He, H. Wang, G. Xiao, B. Yang and B. Hu, *Biosens. Bioelectron.*, 2017, **90**, 343–348.
29 E. Razumienko, O. Ornatsky, R. Kinach, M. Milyavsky, E. Lechman, V. Baranov, M. A. Winnik and S. D. Tanner, *J. Immunol. Methods*, 2008, **336**, 56–63.
30 X. Li, B. Chen, M. He, G. Xiao and B. Hu, *Talanta*, 2018, **176**, 40–46.
31 Y. Zhang, B. Chen, M. He, B. Yang, J. Zhang and B. Hu, *Anal. Chem.*, 2014, **86**, 8082–8089.
32 T. A. Larson, J. Bankson, J. Aaron and K. Sokolov, *Nanotechnology*, 2007, **18**, 325101.
33 G. Sharma, A. Kumar, S. Sharma, M. Naushad, R. P. Dwivedi, Z. A. ALOthman and G. T. Mola, *J. King Saud Univ., Sci.*, 2019, **31**, 257–269.
34 Q. A. Pankhurst, J. Connolly, S. K. Jones and J. Dobson, *J. Phys. D: Appl. Phys.*, 2003, **36**, R167.
35 D. K. Kirui, D. A. Rey and C. A. Batt, *Nanotechnology*, 2010, **21**, 105105.
36 K. Xiong, W. Wei, Y. Jin, S. Wang, D. Zhao, S. Wang, X. Gao, C. Qiao, H. Yue and G. Ma, *Adv. Mater.*, 2016, **28**, 7929–7935.
37 L. Rao, Q. F. Meng, Q. Huang, Z. Wang, G. T. Yu, A. Li, W. Ma, N. Zhang, S. S. Guo and X. Z. Zhao, *Adv. Funct. Mater.*, 2018, **28**, 1803531.
38 A. Parodi, N. Quattrocchi, A. L. Van De Ven, C. Chiappini, M. Evangelopoulos, J. O. Martinez, B. S. Brown, S. Z. Khaled, I. K. Yazdi and M. V. Enzo, *Nat. Nanotechnol.*, 2013, **8**, 61–68.
39 A. Parodi, N. Quattrocchi, A. L. van de Ven, C. Chiappini, M. Evangelopoulos, J. O. Martinez, B. S. Brown, S. Z. Khaled, I. K. Yazdi and M. V. Enzo, *Nat. Nanotechnol.*, 2013, **8**, 61.
40 Z. Chang, Z. Wang, M. Lu, M. Li, L. Li, Y. Zhang, D. Shao and W. Dong, *RSC Adv.*, 2017, **7**, 3550–3553.
41 D. Shao, J. Li, X. Zheng, Y. Pan, Z. Wang, M. Zhang, Q.-X. Chen, W.-F. Dong and L. Chen, *Biomaterials*, 2016, **100**, 118–133.
42 C.-M. J. Hu, L. Zhang, S. Aryal, C. Cheung, R. H. Fang and L. Zhang, *Proc. Natl. Acad. Sci. U. S. A.*, 2011, **108**, 10980–10985.
43 D. Dehaini, X. Wei, R. H. Fang, S. Masson, P. Angsantikul, B. T. Luk, Y. Zhang, M. Ying, Y. Jiang and A. V. Kroll, *Adv. Mater.*, 2017, **29**, 1606209.
44 A. V. Kroll, R. H. Fang and L. Zhang, *Bioconjugate Chem.*, 2017, **28**, 23–32.
45 R. H. Fang, Y. Jiang, J. C. Fang and L. Zhang, *Biomaterials*, 2017, **128**, 69–83.
46 P. L. Rodriguez, T. Harada, D. A. Christian, D. A. Pantano, R. K. Tsai and D. E. Discher, *Science*, 2013, **339**, 971–975.
47 P.-A. Oldenborg, A. Zheleznyak, Y.-F. Fang, C. F. Lagenaur, H. D. Gresham and F. P. Lindberg, *Science*, 2000, **288**, 2051–2054.
48 S. K. Arya, K. Y. Wang, C. C. Wong and A. R. A. Rahman, *Biosens. Bioelectron.*, 2013, **41**, 446–451.
49 Z. Zhang, Q. Luo, X. Yan, Z. Li, Y. Luo, L. Yang, B. Zhang, H. Chen and Q. Wang, *Anal. Chem.*, 2012, **84**, 8946–8951.
50 Y. Pan, M. Guo, Z. Nie, Y. Huang, C. Pan, K. Zeng, Y. Zhang and S. Yao, *Biosens. Bioelectron.*, 2010, **25**, 1609–1614.